Science
AAAS

Villification: How the Gut Gets Its Villi

Amy E. Shyer *et al.*

Science **342**, 212 (2013);
DOI: 10.1126/science.1238842

Science (print ISSN 0036-8075; online ISSN 1095-9203) is published weekly, except the last week in December, by the American Association for the Advancement of Science, 1200 New York Avenue NW, Washington, DC 20005.

Villification: How the Gut Gets Its Villi

Amy E. Shyer,[1]* Tuomas Tallinen,[2,3]* Nandan L. Nerurkar,[1] Zhiyan Wei,[2] Eun Seok Gil,[4] David L. Kaplan,[4] Clifford J. Tabin,[1]† L. Mahadevan[2,5,6,7,8]†

The villi of the human and chick gut are formed in similar stepwise progressions, wherein the mesenchyme and attached epithelium first fold into longitudinal ridges, then a zigzag pattern, and lastly individual villi. We find that these steps of villification depend on the sequential differentiation of the distinct smooth muscle layers of the gut, which restrict the expansion of the growing endoderm and mesenchyme, generating compressive stresses that lead to their buckling and folding. A quantitative computational model, incorporating measured properties of the developing gut, recapitulates the morphological patterns seen during villification in a variety of species. These results provide a mechanistic understanding of the formation of these elaborations of the lining of the gut, essential for providing sufficient surface area for nutrient absorption.

In amniotes, the primitive midgut is established as a cylinder with an outer mesenchymal layer and an inner, luminal endoderm. As development proceeds, distinct radial layers of smooth muscle differentiate. In parallel, the luminal surface of the gut transforms from a smooth surface to a convoluted morphology. In humans, as well as in mice and birds, this leads to an organized array of fingerlike projections termed intestinal villi (*1*, *2*) although a variety of morphologies such as ridges, zigzags, and honeycombs occur in other species (*3*–*5*). Early work suggested a mechanical basis for villus formation (*6*); however, systematic biological or physical studies of this hypothesis are lacking.

Morphogenesis and Differentiation of the Chick Midgut

Until embryonic day 7 (E7), the gut tube, with its inner endodermally derived epithelium and outer mesenchymal layer, maintains a smooth luminal surface (Fig. 1A). At E8, as the first layer of circumferentially oriented smooth muscle begins to form, inward buckling of the tube leads to longitudinal ridges that increase in number until E13, when the differentiation of this layer is complete (Fig. 1B). At this point, a second longitudinally oriented layer of muscle differentiates just exterior to the circular layer, while the previously formed ridges fold into parallel zigzags over 3 days (Fig. 1C). Last, at E16, as a third longitudinally oriented muscle layer differentiates just interior to the circular layer, bulges arise from the

[1]Department of Genetics, Harvard Medical School, Boston, MA 02115, USA. [2]School of Engineering and Applied Sciences, Harvard University, Cambridge, MA 02138, USA. [3]Department of Physics and Nanoscience Center, University of Jyväskylä, FI-40014 Jyväskylä, Finland. [4]Department of Biomedical Engineering, Tufts University, Medford, MA 02155, USA. [5]Department of Organismic and Evolutionary Biology, Harvard University, Cambridge, MA 02138, USA. [6]Department of Physics, Harvard University, Cambridge, MA 02138, USA. [7]Wyss Institute for Biologically Inspired Engineering, Harvard University, Cambridge, MA 02138, USA. [8]Kavli Institute for Nanobio Science and Technology, Harvard University, Cambridge, MA 02138, USA.

*These authors contributed equally to this work.
†Corresponding author. E-mail: lm@seas.harvard.edu (L.M.); tabin@genetics.med.harvard.edu (C.J.T.)

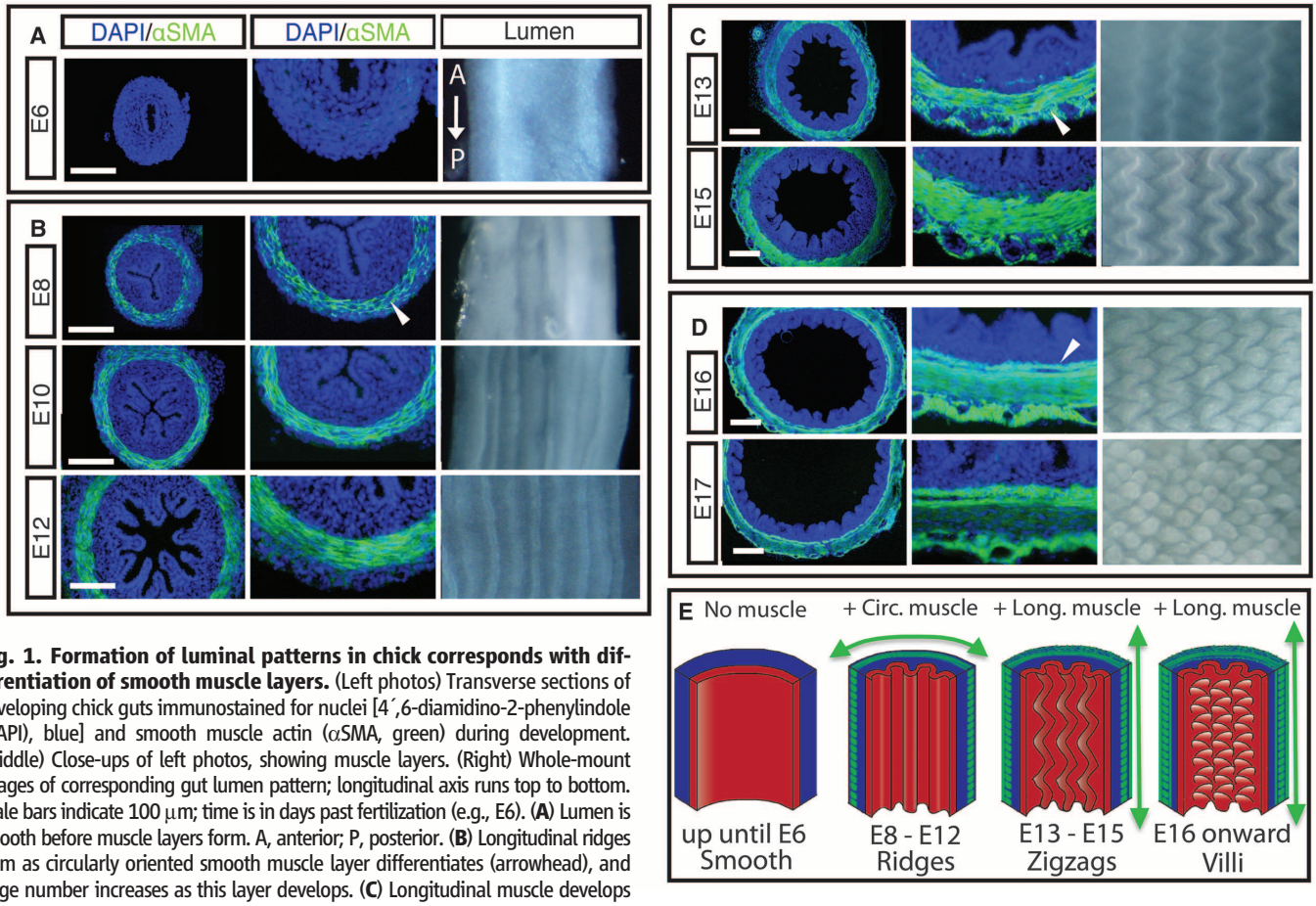

Fig. 1. Formation of luminal patterns in chick corresponds with differentiation of smooth muscle layers. (Left photos) Transverse sections of developing chick guts immunostained for nuclei [4′,6-diamidino-2-phenylindole (DAPI), blue] and smooth muscle actin (αSMA, green) during development. (Middle) Close-ups of left photos, showing muscle layers. (Right) Whole-mount images of corresponding gut lumen pattern; longitudinal axis runs top to bottom. Scale bars indicate 100 μm; time is in days past fertilization (e.g., E6). (**A**) Lumen is smooth before muscle layers form. A, anterior; P, posterior. (**B**) Longitudinal ridges form as circularly oriented smooth muscle layer differentiates (arrowhead), and ridge number increases as this layer develops. (**C**) Longitudinal muscle develops exterior to the circular layer (arrowhead) coincident with the formation of zigzags whose periodicity is maintained but with increasing amplitude and compactness over time. (**D**) A second longitudinal muscle layer forms, interior to the circular layer (arrowhead), coincident with the formation of villi. (**E**) Schematic illustrating the process of muscle differentiation and luminal patterning over time.

zigzag pattern that presage the formation of villi (Fig. 1D). The coincident emergence of luminal ridges, zigzags, and villi with the sequential formation of smooth muscle layers suggests that smooth muscle differentiation and epithelial morphogenesis might be linked.

Ridges Form Because of Muscle-Constrained Azimuthal Growth of the Endoderm-Mesenchyme Composite

The notion that differential growth of layered tissues can lead to epithelial buckling is classical (*7*, *8*) and has been evoked, for example, to explain longitudinal ridge formation in healthy and diseased adult trachea and esophagus (*4*, *9*). To investigate the tissue interactions that lead to the ridge patterns in the embryonic gut, we surgically separated the layers and observed the effects on their respective morphologies. When the muscle was separated from the combined mesenchymal and epithelial layers at different stages from E8, when the circular muscle layer first forms, to E12 just before the first longitudinal muscle layer forms, we found that the mesenchyme and attached epithelium unfold (Fig. 2A). This indicates that relative growth of these layers leads to reversible elastic compression when constrained within the muscle layer; indeed the ratio of the inner circumference of the once-attached muscle layer to the outer circumference of the separated mesenchyme and endoderm, the circumferential stretch ratio, consistently averages to 0.55 across the developmental stages from E8 to E12 (Fig. 2B). However, the separation of the endoderm from the composite of mesenchyme and muscle does not abolish ridge pattern in the mesenchyme (Fig. 2C).

Taken together, these results support a model that the circular muscle layer, once differentiated, forms a stiff constraint mechanically preventing the free azimuthal expansion of the mesenchyme and endoderm; further growth of these tissues relative to the muscle layer leads to azimuthal compression and buckling. This suggests that absent muscle differentiation, the gut tube would expand freely radially without ridge formation. To test this, we developed an in vitro culture system for gut growth. When segments of E6 guts with smooth lumens and no muscle layers were cultured for 48 hours in vitro, they differentiated to form a ring of circumferential smooth muscle and parallel luminal folds, indistinguishable from in ovo E8 guts (Fig. 2D). When E6 guts were cultured in the presence of 10 μM AG1295 or FK506, drugs known to block the differentiation of smooth muscle but that act through distinct signaling pathways (*10*, *11*), they did not form a smooth muscle layer and concomitantly did not form luminal folds (Fig. 2D). Importantly, these compounds did not influence proliferation or lead to an increase in cell death when compared with guts grown with the vehicle (dimethyl sulfoxide, DMSO) alone (fig. S1); indeed there was a significant increase in the outer circumference of guts lacking circular smooth muscle when compared with control gut samples, confirming that blocking smooth muscle differentiation eliminates circumferential restriction of the outward expansion of the gut tube. As a control, gut segments grown in vehicle alone developed a layer of circular smooth muscle and formed luminal folds. Quantifying the constraint provided by the muscle, we find that the ratio of inner circumference of the muscle layer in the control samples to the outer circumference of the gut segments cultured with either compound to be 0.53 on average (Fig. 2D), a ratio that agrees closely with the stretch ratio obtained from surgical separation of the layers, indicating that tissue differentiation into smooth muscle provides most of the circumferential constraint.

Because smooth muscle begins active peristalsis once it forms, the contractility of muscle could drive epithelial buckling in addition to, or instead of, functioning as a passive barrier to expansion. To test this, we cultured E6 gut segments

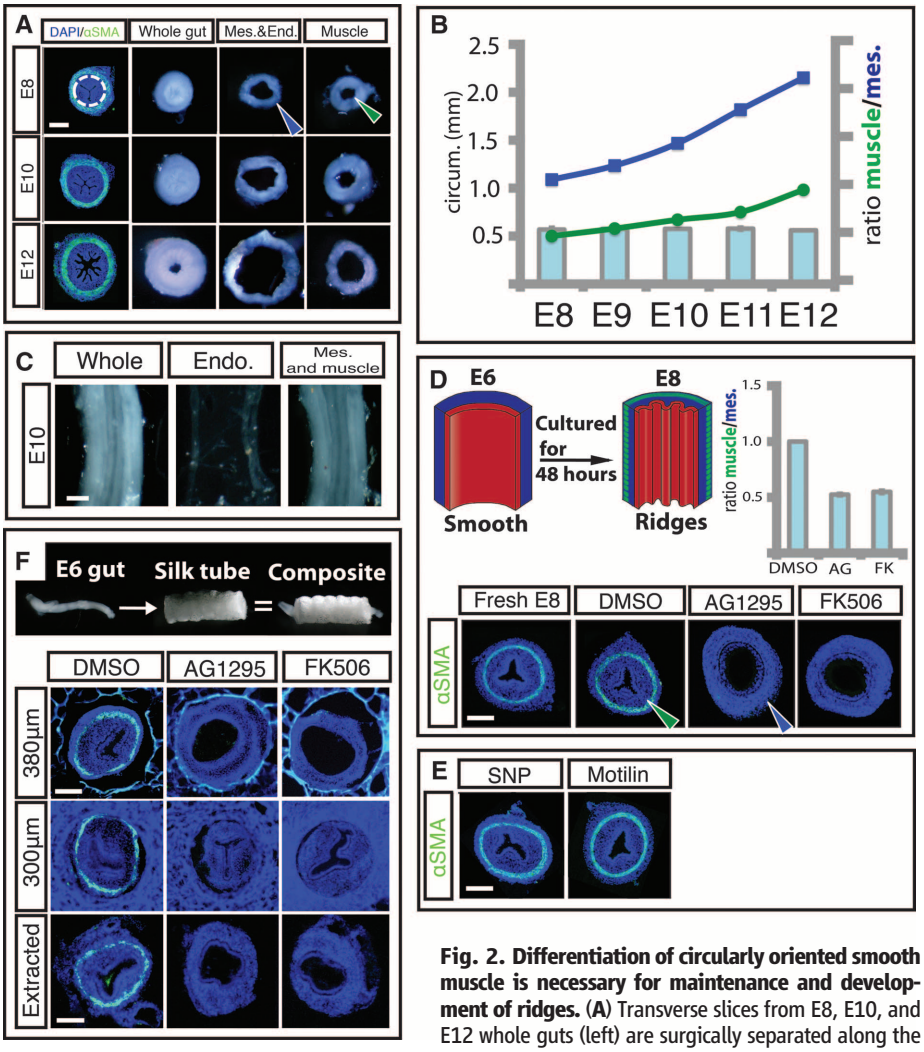

Fig. 2. Differentiation of circularly oriented smooth muscle is necessary for maintenance and development of ridges. (**A**) Transverse slices from E8, E10, and E12 whole guts (left) are surgically separated along the junction of the mesenchyme and the circular smooth muscle (dotted line). When separated from the muscle, the luminal ridges in the mesenchyme and attached endoderm unfold (middle) and expand, whereas the detached muscle remains invariant (right). The outer circumference of the unfolded mesenchyme and endoderm (blue arrowhead) is larger than the inner circumference of the separated muscle layer (green arrowhead). (**B**) Inner circumference of muscle layer (green line) compared with outer circumference of mesenchyme and endoderm (blue line) over time, along with the compression ratio (bar graph). (**C**) Surgical separation of endoderm from mesenchyme and muscle at E10 does not abolish ridge pattern. (**D**) (Top left) Experiment schematic of E6 gut cultured for 48 hours. (Bottom) Transverse sections of a fresh E8 gut or E6 guts cultured in DMSO alone or with either 10 μm AG1295 or 10 μm FK506 for 48 hours and labeled with DAPI (blue) and SMA (green). (Top right) Quantification of compression from E8 muscle shows the ratio of the inner circumference of the circular muscle at E8 (green arrowhead) to the resulting mesenchyme outer circumference (blue arrowhead). (**E**) Transverse sections of guts labeled as in (D); culturing E6 guts in the presence of either SNP or motilin does not affect ridge formation. (**F**) Transverse sections of guts labeled as in (D), cultured in silk tubes of 380-μm inner diameter (top) or 300-μm inner diameter (middle) or cultured in 300 μm and extracted before fixation (bottom). $n > 3$ for all culture experiments; error bars represent one SD. Scale bars = 100 μm.

with either sodium nitroprusside (SNP), a compound shown to inhibit smooth muscle contraction during peristalsis, or motilin, known to enhance peristaltic smooth muscle contraction (*12*, *13*). After 48 hours in culture, neither compound affected the formation of luminal ridges, suggesting that the spontaneous contractility of smooth muscle is not required for epithelial buckling (Fig. 2E).

Last, to assess whether the role of the circular smooth muscle layer as a stiff barrier is sufficient to drive luminal folds, we sought to mimic its role in samples where smooth muscle development was blocked. To do so, we constrained radial gut growth by using porous silk tubes, synthesized by spinning silk fibroin around a reciprocating rotating mandrel with the inner diameter of the circular smooth muscle (*14*). E6 gut segments cultured inside of silk tubes in the presence of either AG1295 or FK506 for 48 hours did not form a muscle layer and, when given sufficient room to expand in silk tubes of 380-μm inner diameter, still did not form luminal ridges (Fig. 2F). However, when the segments were grown in AG1295 and FK506 and restricted by a silk tube of inner diameter of 300 μm, they formed ridges similar to those seen in control guts in spite of the lack of smooth muscle (Fig. 2F). This demonstrates that the mechanical barrier function of the circumferential smooth muscle is sufficient for luminal ridge formation. Moreover, upon removal from the confining silk tube, these ridges were quickly lost, just as they vanished from gut tubes upon surgical removal of the circumferential muscle layer (Fig. 2F), corroborating our previous finding that continued mechanical constraint is required for the maintenance of luminal ridges.

Zigzag Intermediates Form in Response to Additional Muscle-Constrained Longitudinal Growth in Endoderm-Mesenchyme Composite

As described earlier, at E13 a second longitudinally oriented muscle layer forms; simultaneously the ridges buckle into zigzags. Previous work has shown that a thin layer atop an elastic substrate may take on a zigzag topography when it is compressed biaxially (*15*–*17*), suggesting that the longitudinal muscles in conjunction with the previously established circumferential muscle compress the gut biaxially. To investigate whether the longitudinal muscle layer generates longitudinal compression, we surgically separated the muscle layers from the endoderm-mesenchyme composite at different developmental stages. At E12, before longitudinal muscle or zigzags have formed, the separated mesenchyme and attached endoderm have about the same axial length as the muscle to which they were attached (Fig. 3A). However, after longitudinal muscle layer differentiation, at E13, E14, and E15, the ratios of the length of separated muscle to the mesenchyme and endoderm were about 0.75, 0.69, and 0.55, respectively (Fig. 3A), showing that the endoderm-mesenchyme is increasingly compressed longitudinally as this muscle layer forms. Conversely, separation of the endoderm from the mesenchyme and muscle at E14 did not abolish the zigzag pattern, suggesting that this interaction is not required for maintenance of the zigzags (Fig. 3B).

To directly test whether the development of the outer longitudinal layer is required for the formation of zigzags, we resorted again to our in vitro culture system. When E12 gut segments, with a single, circumferential smooth muscle layer and parallel ridges, were cultured for 48 hours, they differentiated a longitudinal smooth muscle layer and underwent morphogenesis to form zigzags, similar to those seen in guts harvested at E14 (Fig. 3C). In the presence of either AG1295 or FK506, the longitudinal muscle layer failed to differentiate, and concomitantly the zigzag pattern did not form, suggesting that the longitudinal layer is required to induce zigzags. These compounds only block further smooth muscle formation and leave established layers intact, so the ridge patterns remain (Fig. 3C). Additionally, when differentiation of this longitudinal muscle was blocked, the length of the gut increased significantly compared with control gut segments; the ratio of the length of control gut segments to those cultured in the presence of either compound was on average 0.66; that is, this longitudinal muscle layer compressed the mesenchyme and attached

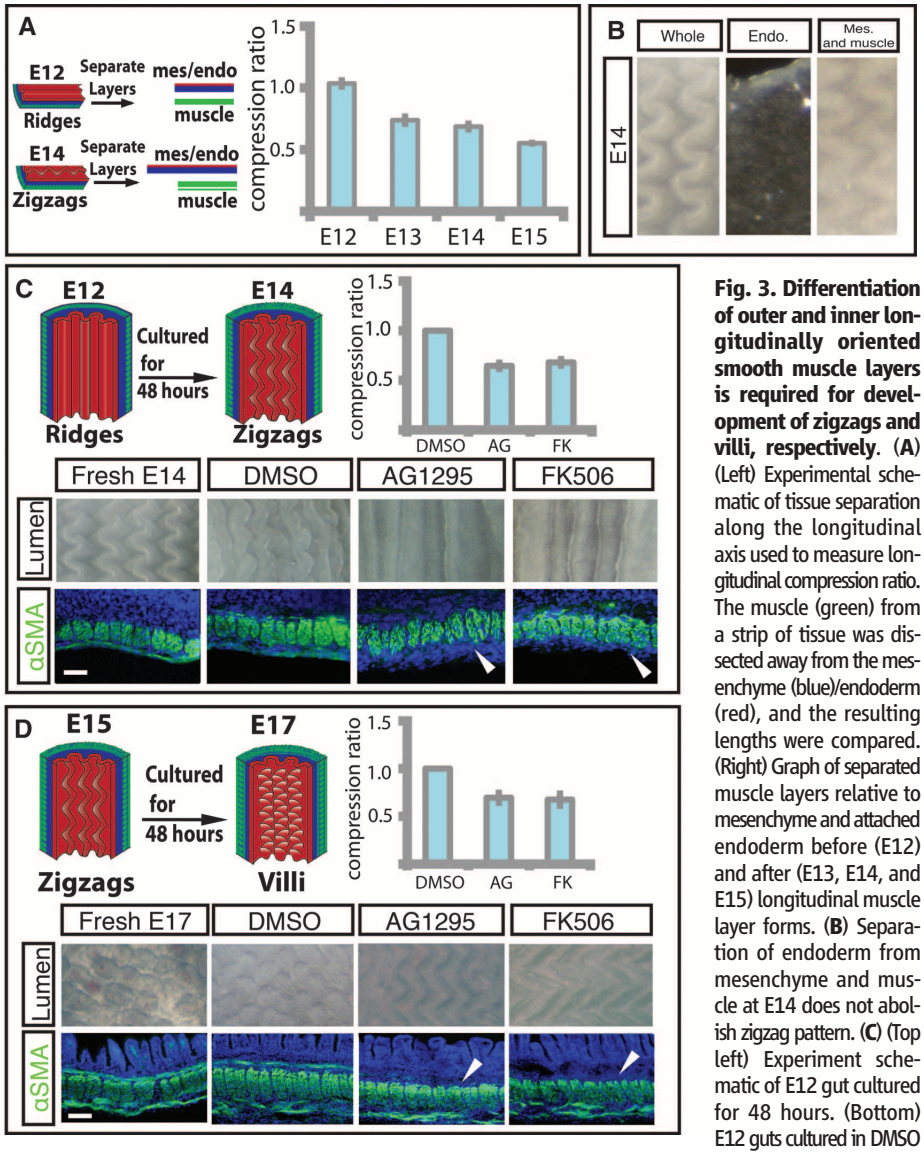

Fig. 3. Differentiation of outer and inner longitudinally oriented smooth muscle layers is required for development of zigzags and villi, respectively. (**A**) (Left) Experimental schematic of tissue separation along the longitudinal axis used to measure longitudinal compression ratio. The muscle (green) from a strip of tissue was dissected away from the mesenchyme (blue)/endoderm (red), and the resulting lengths were compared. (Right) Graph of separated muscle layers relative to mesenchyme and attached endoderm before (E12) and after (E13, E14, and E15) longitudinal muscle layer forms. (**B**) Separation of endoderm from mesenchyme and muscle at E14 does not abolish zigzag pattern. (**C**) (Top left) Experiment schematic of E12 gut cultured for 48 hours. (Bottom) E12 guts cultured in DMSO alone or with either 10 μm AG1295 or 10 μm FK506 for 48 hours. Middle photos show luminal views, and bottom photos show longitudinal sections labeled with DAPI (blue) and SMA (green). Arrowheads denote absence of muscle layer. (Top right) Quantification of compression from E14 longitudinal muscle characterized by the ratio of the length of the control cultured segments to those lacking muscle. (**D**) (Top left) Experiment schematic of E15 gut cultured for 48 hours. (Bottom) Fresh E17 gut or E15 guts cultured in DMSO alone or with either 10 μm AG1295 or 10 μm FK506 for 48 hours. Middle photos show luminal views and bottom photos show longitudinal sections, labeled as in (C). Arrowheads denote absence of muscle layer. (Top right) Quantification of compression from E16 longitudinal muscle, as in (C). $n > 3$ for all culture experiments; error bars represent one SD. Scale bars = 20 μm.

epithelium by a factor of about 1.5 (Fig. 3C). This is consistent with the value obtained by manual dissection of the layers. Just as for ridge formation, transformation of ridges to zigzags is independent of smooth muscle contractility (fig. S2).

Villification Requires a Third Regime of Smooth Muscle Differentiation

To investigate the dependence of the final patterning of villi on the differentiation of the inner, longitudinal smooth muscle layer, we cultured E15 guts, with both a circumferential layer and outer longitudinal layer, for 48 hours in the presence of the muscle-blocking compounds or with the vehicle (DMSO) alone. Although gut segments cultured with DMSO developed a third inner longitudinal muscle layer and formed villi, those cultured with either AG1295 or FK506 failed to form this muscle layer and did not initiate villi (Fig. 3D). When differentiation of this longitudinal muscle was blocked, the length of the tube increased significantly compared with those of control gut segments (Fig. 3D). The ratio of the length of control gut segments to that of those lacking the outer longitudinal muscle was on average 0.68; that is, this muscle layer compressed the mesenchyme and endoderm again by a factor of about 1.5 (Fig. 3D).

All together, our surgical manipulations and drug studies support the hypothesis that differentiating smooth muscle acts as a barrier to the expansion of the attached mesenchyme and endoderm, compressing these layers first circumferentially to form ridges, then longitudinally to form zigzags, and last longitudinally again to form villi. We emphasize that, because the patterns relax when the muscular constraints are released surgically, it follows that the morphology of the lumen is a simple consequence of elastic energy minimization during the constrained growth of a soft, layered elastic tissue.

Mathematical Models Quantify the Role of Tissue Growth Constrained by Muscle Layers to Drive Ridge and Zigzag Formation

To further quantify these luminal patterns, we constructed a mathematical and computational model of the process based on measured geometrical and biophysical parameters. Our models are similar in spirit to recent theoretical approaches to gut luminal patterning based on the hypothesis of differential growth (*18*, *19*) but go beyond them by correctly accounting for the constraints provided by the combination of muscular differentiation and differential growth that we see evidence for, the cylindrical geometry of the gut, and the experimentally measured geometrical and physical properties of the system.

We start by considering a composite of naturally flat elastic mesenchyme and endoderm sheets that are attached together and bent and squeezed to fit into a rigid tubular configuration of inner diameter D that mimics the circular muscle layer (Fig. 4A). We assume that the tissues may be well described by using a simple neo-Hookean constitutive model, with a volumetric strain energy density $W = \frac{1}{2}\mu[\mathrm{Tr}(\mathbf{F}\mathbf{F}^{\mathrm{T}}).J^{-2/3} - 3] + K(J - \log J - 1)$, where μ and K are the shear and bulk moduli, respectively; $\mathbf{F}$ is the elastic deformation gradient; and $J = \det(\mathbf{F})$. Over the multiday time scale of villification, the tissues are assumed compressible with $K = 3\mu$. At each stage, we minimize the elastic energy of the system by using a custom finite element model (supplementary materials). We characterize growth by using the experimentally measured growth parameters, including the outer circumference, $S_0 = \pi D$, of the compressed endoderm-mesenchyme composite, as well as the circumference and thickness of the endoderm and mesenchyme (Fig. 4B and fig. S7). The simulated domain has length $L = 1.25D$ in the longitudinal direction with periodic boundary conditions at the ends, allowing uniform relative longitudinal growth of the layers to develop

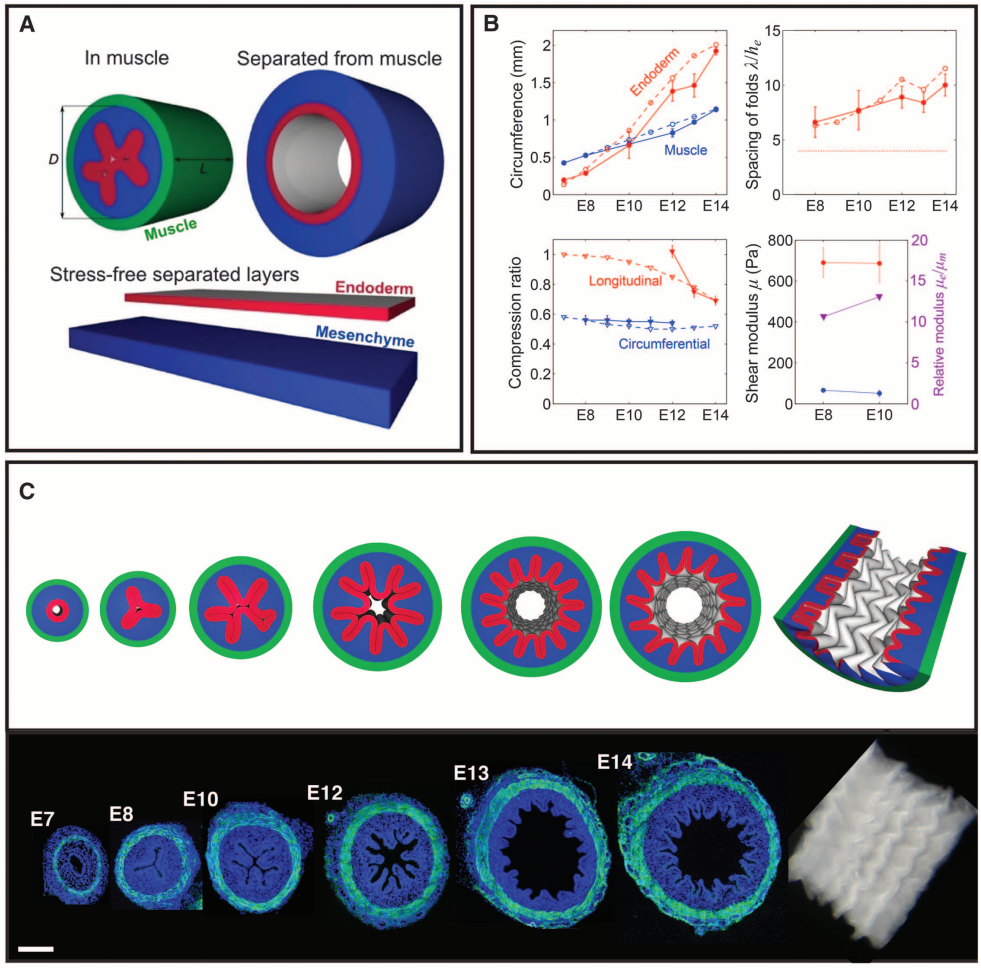

Fig. 4. A numerical simulation predicts the formation of ridges and zigzags in chick gut lumen. (**A**) The model is illustrated by showing the mesenchyme (blue) and the endoderm (red) enclosed in a muscle (green), without muscle, and separated in their stress-free states. (**B**) (Top left) Circumference of the inner boundary of the muscle and endoderm. (Top right) Spacing of longitudinal folds measured along the endoderm and scaled by its thickness. The thin dashed line is the stress-free thickness of the endoderm-mesenchyme composite. (Bottom left) Ratio of muscle to separated endoderm-mesenchyme composite in circumferential and longitudinal directions. (Bottom right) Shear modulus of mesenchyme and endoderm, and their ratio. In all graphs, solid lines correspond to experimental observations and dashed lines to the computational model. Error bars, 1 SD. (**C**) A simulation shows ridge-folds forming due to circumferential compression, followed by buckling into a zigzag pattern due to longitudinal compression. Sections of corresponding chick guts labeled with DAPI (blue) and SMA (green) are shown below.

axial compression that mimics the role of the longitudinal muscles at E13 and E14 when zigzags arise. With the geometrical parameters (full details in the supplementary materials) and the measured elastic moduli of the tissues (Fig. 4B and figs. S3 to S6) that show that the endoderm is about 10 times stiffer than the mesenchyme, our simulations allow us to follow the evolution of luminal patterning shown in Fig. 4C and movie S1. We see that both ridge and zigzag patterns arise as mechanical instabilities in the constrained growing tissue that sequentially break circumferential and then longitudinal symmetry in the gut with a wavelength and amplitude comparable to the thickness of the endoderm-mesenchyme composite (Fig. 4B).

Villification Also Requires Localized Changes in Endodermal and Mesenchymal Proliferation in Addition to Smooth Muscle Differentiation

Although additional compression from the inner longitudinal layer is necessary for the formation of villi from zigzags, as shown in Fig. 3, longitudinal compression alone is not sufficient to effect this transformation (fig. S9A).

Previous work in mouse has shown that, although proliferating cells can be found uniformly across the mesenchyme and endoderm before villi arise, as villi form, proliferating cells are found only in the intervillous region (*2*). Similarly, in chick guts, proliferating cells appear uniformly within each tissue layer through the formation of zigzags (Fig. 5 and fig. S8), but at E15, after zigzags form and just before villi arise, proliferating cells are found predominantly in the valleys between the raised zigzags (Fig. 5A). However, once villi begin to form at E16, proliferation is no longer restricted from the tips (Fig. 5A). Additionally we find that in vitro 5-ethynyl-2′-deoxyuridine (EdU) pulse labeling of E15 gut samples results in labeled cells at the sides and tips of forming villi, suggesting that these changes in proliferation patterns may reflect a displacement of the dividing cells upward from the valleys as the luminal topography shifts from zigzags to villi. Specifically, each "arm" of the zigzag twists out of the plane and into the lumen, pinching off a region of the zigzag arm near each "elbow," delineating pockets of mesenchyme surrounded by endoderm, each of which becomes a villus (Fig. 5B).

To understand how the topographical changes during zigzag twisting might relocate regions of proliferation as villi form, we created a clay model of zigzags. Labeling the proliferating regions of our model zigzags and manually twisting them mimics the twist observed in the E16 gut (Fig. 5C). Furthermore, the resulting clay label localization closely matches EdU staining for proliferation in the sectioned E16 gut tissue (Fig. 5C), suggesting that these tissue movements account for the observed proliferation patterns as villi form.

To probe the effect of nonuniform growth in our computational model, we set up a minimal planar configuration of mesenchyme and endoderm (supplementary materials, fig. S9, and movie S2). Initially, the endoderm and mesenchyme are assumed to have nominal compression ratios of 0.5 and 0.6, respectively, in both lateral directions, as measured experimentally (Fig. 3A). This results in a tightly packed zigzag pattern (fig. S9A), with a spacing of twice the thickness of the endoderm-mesenchyme composite in both directions, in agreement with experiments. By using our experimental observations of nonuniform proliferation as guides, we incorporate nonuniform growth to this pattern by allowing the growth of spots of the endoderm in the zigzag valleys, centered at the deepest points of the valleys, with lateral diameter six times the endoderm thickness. These spots are grown laterally until their diameter doubles during the simulation relative to areas of the endoderm outside the spots. This pattern of growth causes the zigzags to shift and twist so as to relocate the rapidly growing regions to the arms, similar to our clay model. As the spots relieve their growth strain at the arms, they form previllous bulges (Fig. 5E). Sliced plane views of this twisted pattern reveal their similarity to the corresponding experimental patterns (Fig. 5F); bulging peaks are rotated,

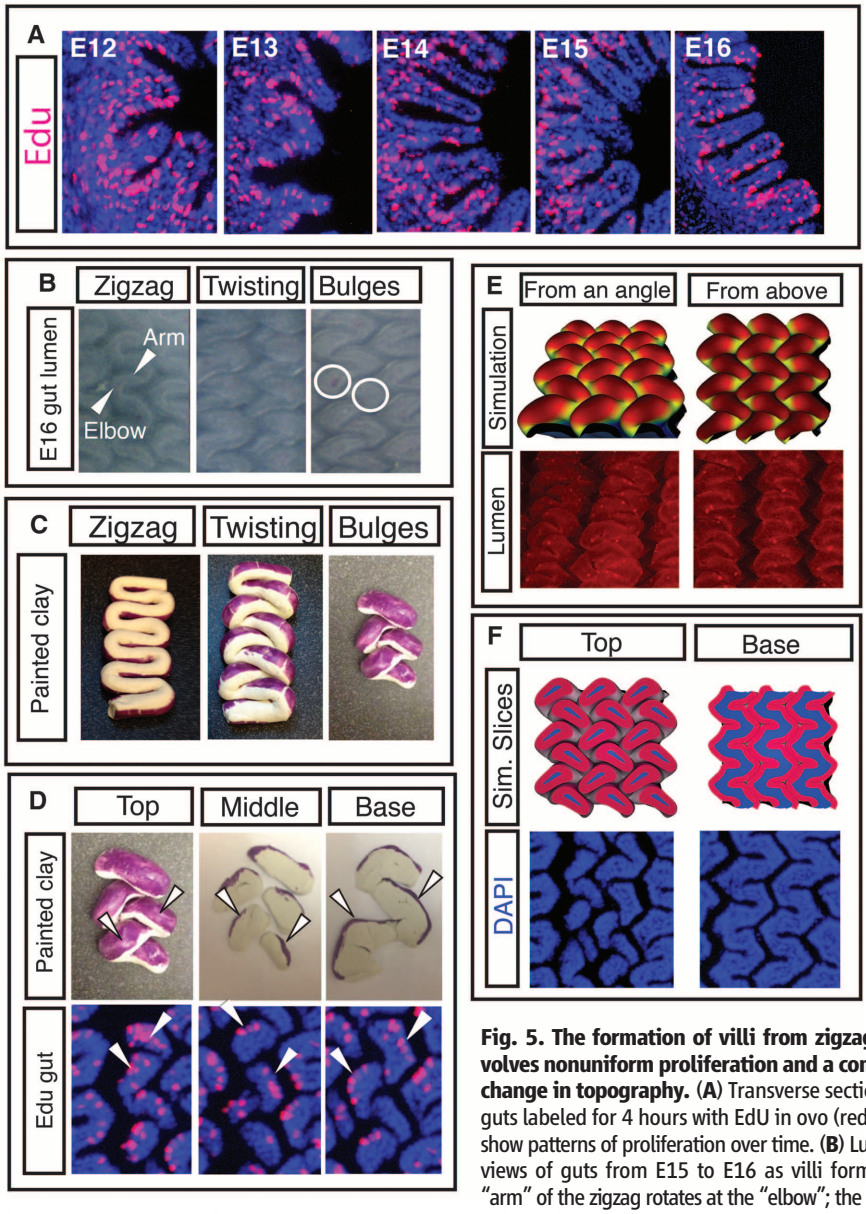

Fig. 5. The formation of villi from zigzags involves nonuniform proliferation and a complex change in topography. (**A**) Transverse sections of guts labeled for 4 hours with EdU in ovo (red) guts show patterns of proliferation over time. (**B**) Luminal views of guts from E15 to E16 as villi form. The "arm" of the zigzag rotates at the "elbow"; the circles denote the resulting pockets of mesenchyme surrounded by endoderm that will each become a villus. (**C**) Clay models; purple label represents proliferating regions. Clay model is twisted to mimic change in topography seen in (B). (**D**) (Top) Labeled, twisted model of E16 gut is sliced with a razor blade to reveal label localization. (Bottom) EdU label in longitudinal sections of E16 guts; arrowheads highlight similarity of pattern. (**E**) (Top) A simulation that incorporates nonuniform proliferation along with measured geometrical and biophysical parameters shows villi morphogenesis. (Bottom) Corresponding images of the chick lumen (red color and stained puncta are due to antibody stain and should be disregarded). (**F**) (Top) Sections of the simulations in (D). (Bottom) Corresponding sections in chick.

whereas the regular zigzag valleys persist deeper in the pattern.

Thus, although the final patterning step where definitive villi arise involves more complex morphogenesis and nonuniform proliferation, it follows from the same general physical principle: Differential growth in a constrained environment leads to buckling and folding patterns as circumferential, longitudinal, and eventually radial symmetry are broken sequentially.

A Phylogenetically Conserved Mechanism Directs Luminal Gut Morphogenesis

Although the patterns seen on the luminal surface of the gut vary substantially across species (fig. S10), the underlying physical principles we have uncovered for the chick lumen morphology suggest that similar mechanisms operate broadly.

In the adult *Xenopus*, the luminal surface of the intestine is folded into a zigzag pattern (*4*). Development of this pattern involves progressing through the same patterning steps as in chick, with a smooth lumen forming ridges that then develop into zigzags via identical mechanisms (Fig. 6A). However, *Xenopus*, unlike chick, does not develop the second inner longitudinal muscle layer (Fig. 6A); the absence of this muscular layer, and thence the absence of additional compression, explains why individual villi do not develop in *Xenopus*. Our computational models can account for the differences in zigzags between *Xenopus* and chick, as well as more exotic patterns seen in snakes (supplementary materials and fig. S10).

In the mouse, the gut does not progress through ridges and zigzags; instead, villi emerge directly from a smooth lumen (*20*). Although these villi arise only once smooth muscle layers form, the layers differentiate much more rapidly in mouse than in chick (Fig. 6E). This suggests that the relatively quick pace at which muscle layers form in the mouse does not leave time for proliferation and expansion of the inner mesenchyme and endoderm between the differentiation of sequential muscle layers and thus prevents the development of visible intermediate patterns such as ridges and zigzags. Specifically, all muscle layers develop within a 48-hour period, a short time compared with the 8 days required for muscle to fully develop in chick (*20*). To experimentally determine whether villus formation in mouse also requires differentiation of smooth muscle, we tested the effect of the smooth muscle inhibitors used in our chick studies on the formation of villi in mouse guts grown in culture. Just as in chick, the mouse guts grown in the presence of AG1295 or FK506 did not form smooth muscle and concomitantly did not develop villi (Fig. 6B), suggesting that compression from the smooth muscle layer is necessary for, and drives the formation of, villi in mouse.

Our studies are in sharp contrast to a recent view of mouse gut patterning that postulates a potential inductive role of the endodermally derived signal Sonic hedgehog (Shh) in triggering a morphogenetic cascade directing villus outgrowth (*21*). The key results that led in this direction were the failure of villus formation when Shh activity was pharmacologically blocked with the Shh antagonist cyclopamine and the increased size of the villi when guts were provided with excess Shh signal. However, because these reagents were applied before villus formation, they were de facto also treated before smooth muscle differentiation. Because Shh activity is both necessary and sufficient to direct smooth muscle formation in the developing intestine (*22*, *23*), an alternative explanation would be that cyclopamine, by preventing smooth muscle specification, eliminates the constraint necessary for villi to form, consistent with our current studies.

To quantitatively test our theory of villification in the mouse gut, we performed mechanical

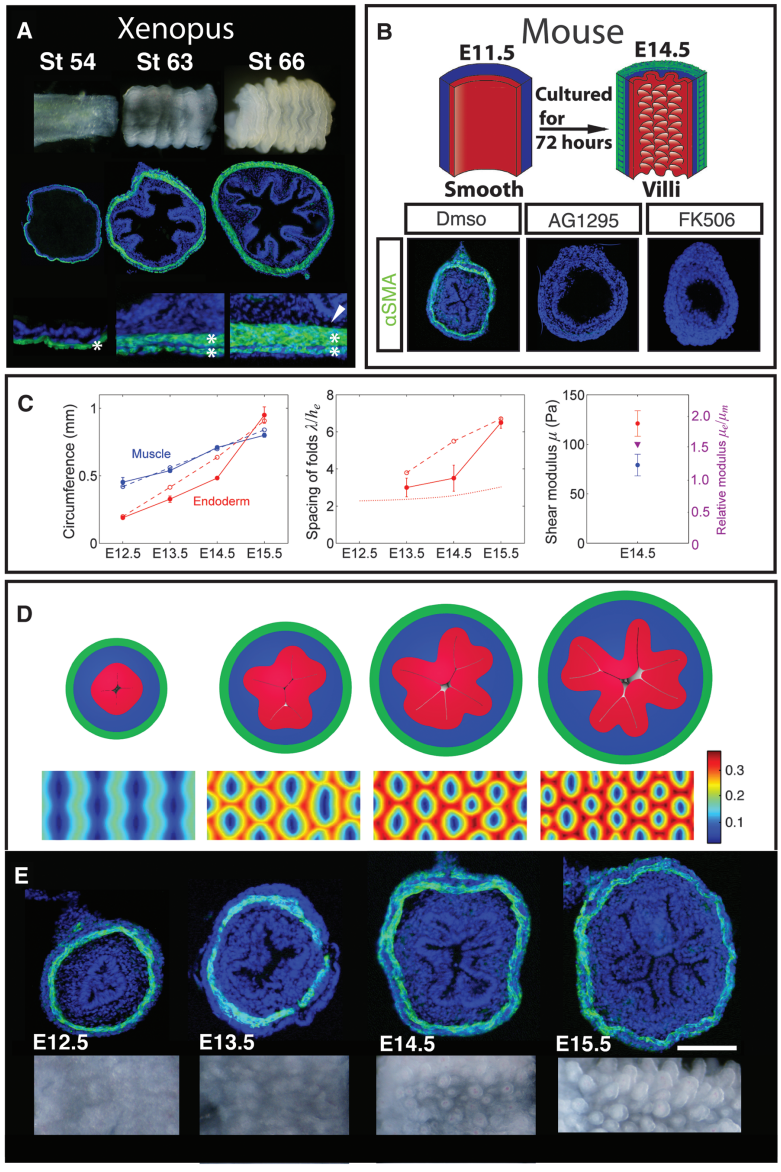

Fig. 6. The physical mechanism of villification can be extended to other species. (**A**) Luminal pattern formation in *Xenopus*. Sections labeled with DAPI (blue) and SMA (green). The circumferential and outer longitudinal layers form (asterisks), but the inner longitudinal layer does not form (arrowhead). (**B**) Transverse sections of E11.5 mouse guts [labeled as in (A)] cultured in vehicle alone (DMSO) or with either 10 μm AG1295 or 10 μm FK506 for 72 hours; experiment schematized above. (**C**) (Left) Circumference of the inner boundary of the muscle and endoderm. (Middle) Spacing of folds measured along the endoderm and scaled by its thickness. Dotted line is the stress-free thickness of the endoderm-mesenchyme composite. (Right) Shear moduli of mesenchyme and endoderm and their ratio. In all graphs, solid lines correspond to experimental observations and dashed lines to simulations. (**D**) Cross-sectional (top) and luminal (bottom) images from a simulation based on measurements from the developing mouse gut. Color shows distance of the luminal surface to the center line, relative to the diameter of the tube. (**E**) Transverse sections [labeled as in (A)] and whole-mount images of the lumen for corresponding stages during mouse villi formation. $n > 3$ for culture experiments; error bars represent one SD. Scale bars = 100 μm.

and morphometric measurements of the tissues in the developing mouse gut (Fig. 6C). Using these measurements as inputs in our model suffices to quantitatively predict the formation of villi (supplementary materials, Fig. 6D, and movie S3). Compared with the chick, where the endoderm is more than 10 times stiffer than the adjacent mesenchyme, the mouse endoderm is only about 1.5 times as stiff as the mesenchyme (fig. S3). Our simulations show that the soft endoderm in mouse is essential for the initial folding that occurs in endoderm alone and for the direct formation of an array of previllous bumps, rather than zigzags, which are qualitatively similar to sulcus formation on biaxially compressed gel surfaces that lack a stiff top layer (*24*). The spacing of bumps and, consequently, the spacing of villi are comparable to the thickness of the whole endoderm-mesenchyme composite (Fig. 6C), similar to chick.

The process of villification occurs before the differentiation of the gut endoderm into various epithelial cell types (*25*–*27*) and well before the postnatal process of crypt formation. In vitro culture of intestinal stem cells results in the formation of intestinal organoids that reproduce crypt structure (*28*). These organoids consist of an inner epithelium with villuslike cell types and outwardly projecting cryptlike structures. However, no morphological structures are present in these in vitro cultures resembling the physical villi. These results suggest that crypt formation likely does not require the same muscle-driven compression that is necessary for villi to form.

Additionally, further study is needed to understand whether structural differences in the lumen of different regions of the gut are attributable to distinctions in the parameters we have measured. For example, the short, wide villi that coat large longitudinal folds of the chick colon may be attributable to the thicker muscle layers of the colon. Consistent with the muscle playing such a role, studies have shown that transposition of a ring containing all radial layers of the colon into regions of the small intestine preserve villi morphology (*29*).

Our previous work provided a mechanical basis for the diversity of macroscopic looping patterns of the gut based on geometry, differential growth, and tissue mechanics (*30*), and our present results demonstrate that the same physical principles drive morphological variation on the luminal surface of the gut. Further, we see that relatively minor changes in the geometry, growth, and physical properties of the developing tissue in the guts of various species can substantially alter both the process and the form of villus patterning. A deep understanding of how patterns vary requires us to combine our knowledge of biophysical mechanisms with the genetic control of cell proliferation and growth; indeed this variation can occur in an organism as a function of its diet, across species, and over evolutionary time scales via natural selection.

References and Notes

1. V. A. McLin, S. J. Henning, M. Jamrich, *Gastroenterology* **136**, 2074–2091 (2009).
2. T. K. Noah, B. Donahue, N. F. Shroyer, *Exp. Cell Res.* **317**, 2702–2710 (2011).
3. W. J. Krause, *Anat. Histol. Embryol.* **40**, 352–359 (2011).
4. J. W. McAvoy, K. E. Dixon, *J. Anat.* **125**, 155–169 (1978).
5. S. Ferri, L. C. U. Junqueira, L. F. Medeiros, L. O. Mederios, *J. Anat.* **121**, 291–301 (1976).
6. D. R. Burgess, *Embryol Exp. Morph.* **34**, 723–740 (1975).
7. W. His, *Anatomie Menschlicher Embryonen* (Vogel, Leipzig, Germany, 1880).
8. D. E. Moulton, A. Goriely, *J. Mech. Phys. Solids* **59**, 525–537 (2011).
9. L. Bell, L. Williams, *Anat. Embryol.* **165**, 437–455 (1982).
10. M. Kurahashi *et al.*, *Neurogastroenterol. Motil.* **20**, 521–531 (2008).
11. K. Fukuda, Y. Tanigawa, G. Fujii, S. Yasugi, S. Hirohashi, *Development* **125**, 3535–3542 (1998).
12. H. Benabdallah, D. Messaoudi, K. Gharzouli, *Pharmacol. Res.* **57**, 132–141 (2008).
13. N. Harada, Y. Chijiiwa, T. Misawa, M. Yoshinaga, H. Nawata, *Life Sci.* **51**, 1381–1387 (1992).
14. M. L. Lovett, C. M. Cannizzaro, G. Vunjak-Novakovic, D. L. Kaplan, *Biomaterials* **29**, 4650–4657 (2008).
15. N. Bowden, S. Brittain, A. G. Evans, J. W. Hutchinson, G. W. Whitesides, *Nature* **393**, 146–149 (1998).
16. L. Mahadevan, S. Rica, *Science* **307**, 1740 (2005).
17. B. Audoly, A. Boudaoud, *J. Mech. Phys. Solids* **56**, 2444–2458 (2008).
18. E. Hannezo, J. Prost, J.-F. Joanny, *Phys. Rev. Lett.* **107**, 078104 (2011).
19. M. Ben Amar, F. Jia, *Proc. Natl. Acad. Sci. U.S.A.* **110**, 10525–10530 (2013).
20. R. Sbarbati, *J. Anat.* **135**, 477–499 (1982).
21. K. D. Walton *et al.*, *Proc. Natl. Acad. Sci. U.S.A.* **109**, 15817–15822 (2012).
22. A. Sukegawa *et al.*, *Development* **127**, 1971–1980 (2000).
23. M. Ramalho-Santos, D. A. Melton, A. P. McMahon, *Development* **127**, 2763–2772 (2000).
24. T. Tallinen, J. S. Biggins, L. Mahadevan, *Phys. Rev. Lett.* **110**, 024302 (2013).
25. M. Dauça *et al.*, *Int. J. Dev. Biol.* **34**, 205–218 (1990).
26. Z. Uni, A. Smirnov, D. Sklan, *Poult. Sci.* **82**, 320–327 (2003).
27. F. T. Bellware, T. W. Betz, *J. Embryol. Exp. Morphol.* **24**, 335–355 (1970).
28. T. Sato *et al.*, *Nature* **459**, 262–265 (2009).
29. W. H. St. Clair, C. A. Stahlberg, J. W. Osborne, *Virchows Arch. B Cell Pathol. Incl. Mol. Pathol.* **47**, 27–33 (1984).
30. T. Savin *et al.*, *Nature* **476**, 57–62 (2011).

Acknowledgments: We thank M. Kirschner for providing *Xenopus* tadpoles and O. Pourquie for providing snake embryos. D.L.K. and Tufts University hold a series of patents that cover the processing of silk into material structures, including those used in the research reported here. T.T. acknowledges the Academy of Finland for support. Computations were run at CSC–IT Center for Science, Finland. C.J.T. acknowledges the support of a grant from NIH RO1 HD047360. L.M. acknowledges the support of the MacArthur Foundation.

Supplementary Materials

www.sciencemag.org/content/342/6155/212/suppl/DC1
Materials and Methods
Supplementary Text
Figs. S1 to S11
Movies S1 to S3

8 April 2013; accepted 13 August 2013
Published online 29 August 2013;
10.1126/science.1238842

REPORTS

Evidence for Water in the Rocky Debris of a Disrupted Extrasolar Minor Planet

J. Farihi,[1]* B. T. Gänsicke,[2] D. Koester[3]

The existence of water in extrasolar planetary systems is of great interest because it constrains the potential for habitable planets and life. We have identified a circumstellar disk that resulted from the destruction of a water-rich and rocky extrasolar minor planet. The parent body formed and evolved around a star somewhat more massive than the Sun, and the debris now closely orbits the white dwarf remnant of the star. The stellar atmosphere is polluted with metals accreted from the disk, including oxygen in excess of that expected for oxide minerals, indicating that the parent body was originally composed of 26% water by mass. This finding demonstrates that water-bearing planetesimals exist around A- and F-type stars that end their lives as white dwarfs.

The enormous recent progress in the discovery of exoplanetary systems provides a growing understanding of their frequency and nature, but our knowledge is still limited in many respects. There is now observational evidence of rocky exoplanets (*1*, *2*), and the mass and radius (and hence density) of these planets can be calculated from transit depth and radial velocity amplitude; however, estimates of their bulk composition remain degenerate and model-dependent. Transit spectroscopy offers some information on giant exoplanet atmospheres (*3*), and planetesimal debris disks often reveal the signature of emitting dust and gas species (*4*), yet both techniques only scratch the surface of planets, asteroids, and comets. Interestingly, white dwarfs—the Earth-sized embers of stars like the Sun—offer a unique window onto terrestrial exoplanetary systems: These stellar remnants can distill entire

[1]Institute of Astronomy, University of Cambridge, Cambridge CB3 0HA, UK. [2]Department of Physics, University of Warwick, Coventry CV5 7AL, UK. [3]Institut für Theoretische Physik und Astrophysik, University of Kiel, 24098 Kiel, Germany.

*Corresponding author. E-mail: jfarihi@ast.cam.ac.uk